as its one arm,[15] in-fiber Mach-Zehnder interferometer using interference between guided mode and clad mode,[16,17] side-by-side coupled microfibers,[18] a graphene-covered optical prism,[8] a graphene-coated microfiber, a graphene-covered D-shape fiber.[8,19] Micro-ring resonator covered with graphene has been investigated from the viewpoint of resonant quality[20] and optical modulation.[21] Microring resonators[22] have also been used for sensing without graphene layer.[23–25]

In this paper, we propose a gas sensor consisting of graphene covered silicon-waveguide microring resonator for NH_3 gas.[26] Since the optical wavelength used for sensing is in optical communication band, remote sensing through optical fiber transmission is performed without electro-magnetic affection. It is found that the gas concentration can be detected by the resonant wavelength change. The Fermi energy is manipulated by applying voltage to the graphene, which will result in adjusting the sensing sensitivity and the sensing range of gas concentration. We discuss comprehensive description of the sensing principle and detailed derivation of equations based on our proposal.[26] The optical sensing with graphene and waveguide devices have advantages such as miniaturized system with small footprint, low power consumption, remote sensing, high-sensitivity, and good flexibility[27] compared to the frequently used techniques in commercial NH_3 gas detectors based on metal- and semiconductor-oxide sensors, catalytic metal sensors, conducting polymer sensors, and optical absorbance analyzers.[28]

2. Device structure

The basic structure of the proposed device consists of a microring resonator with ring radius R covered by a single atomic layer of graphene as shown in Fig. 1. The graphene is assumed to coat on top and side surfaces of the ring waveguide and on the substrate. Optical continuous wave at wavelength λ is coupled from a straight waveguide. The silicon waveguides with width W and height H are formed on a SiO_2/Si substrate. The fabrication process described in Ref.[20] is a possible way for our proposed device. Selective patterning of graphene is also described in the literature, which is performed by reactive ion etching with an O_2 gas flow.

NH_3 molecules adsorbed on graphene will act like a donor.[5,8] As a result, the adsorption of NH_3 molecules changes the Fermi level of the graphene, which induces the conductivity change. High sensitivity is caused by the fact that graphene has a low density of states near the Dirac point and small change in carrier density results in large change in Fermi energy.[14] The resonant wavelength shift in the microring resonator is then induced due to the effective index change of the graphene covered waveguide.

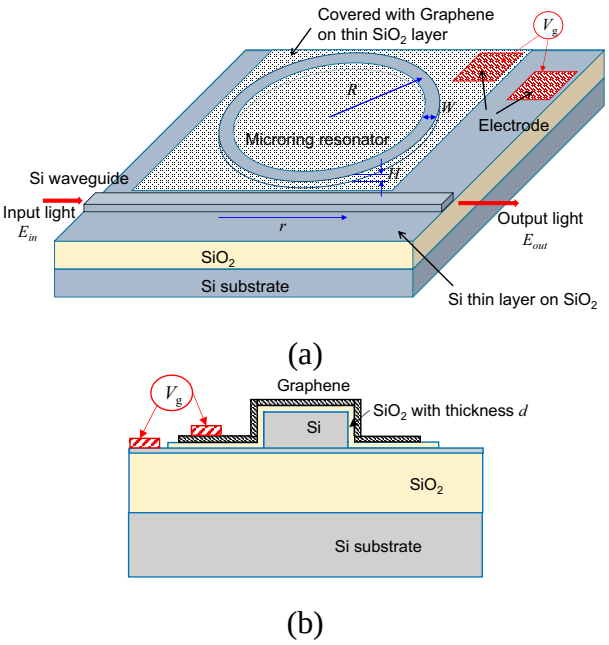

Fig. 1. (a) Graphene covered optical microring-resonator gas sensor and (b) cross-section of the ring resonator with applied voltage.

The Fermi energy is also adjustable by applying voltage to the graphene as shown in Fig. 1(b). The voltage V_g is applied between the graphene and Si waveguide through a thin insulating layer of SiO_2 with thickness d. A thin Si layer is employed below the Si core to apply V_g.[21] Thus, the applied voltage will expect to control the sensitivity and the sensing range of the gas concentration.

3. Sensitivity for NH_3 gas concentration

Assuming the resistivity and the conductivity of graphene without NH_3 gas as ρ_s and σ_s, respectively, we find $\Delta\sigma/\sigma_s = (\Delta\rho/\rho_s)/[(\Delta\rho/\rho_s) + 1]$. Graphene relative resistivity change $\Delta\rho/\rho_s$ as a function of NH_3 concentration is found from the experimental result of resistivity by Yavari *et al.*[29] as shown in Fig.2. The relative conductivity change $\Delta\sigma/\sigma_s$ calculated from the resistivity change is also plotted.

The complex conductivity σ in the graphene is related to Fermi energy μ_c by[30]

$$\sigma(\omega) = \frac{\sigma_0}{2}\left(\tanh\frac{\hbar\omega + 2\mu_c}{4k_BT} + \tanh\frac{\hbar\omega - 2\mu_c}{4k_BT}\right) - j\frac{\sigma_0}{2\pi}\ln\left[\frac{(\hbar\omega + 2\mu_c)^2}{(\hbar\omega - 2\mu_c)^2 + (2k_BT)^2}\right] + j\frac{4\sigma_0}{\pi}\frac{\mu_c}{\hbar\omega + j\hbar\gamma}, \quad (1)$$

where $\sigma_0 = q^2/(4\hbar)$, q is the electron charge, k_BT is the thermal energy, $\hbar\omega$ is the photon energy, $\hbar\gamma$ is the electron relaxation energy, and γ is the intraband scattering rate. The complex

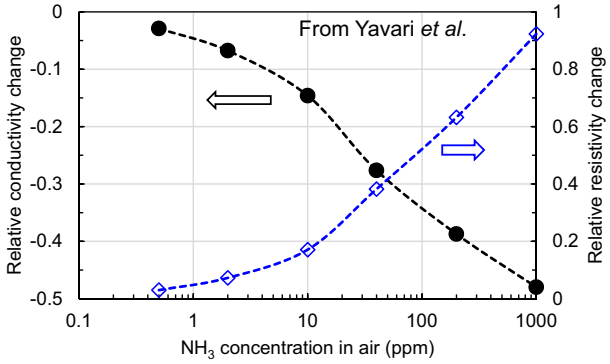

Fig. 2. Resistivity and conductivity of graphene as a function of NH_3 gas concentration from Yavari *et al.*[29)]

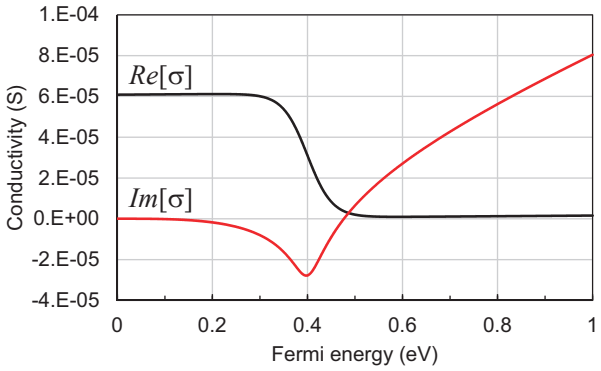

Fig. 3. The complex conductivity $\sigma = \sigma' + j\sigma''(= Re[\sigma] + jIm[\sigma])$ as a function of the Fermi energy μ_c using eq.(1).

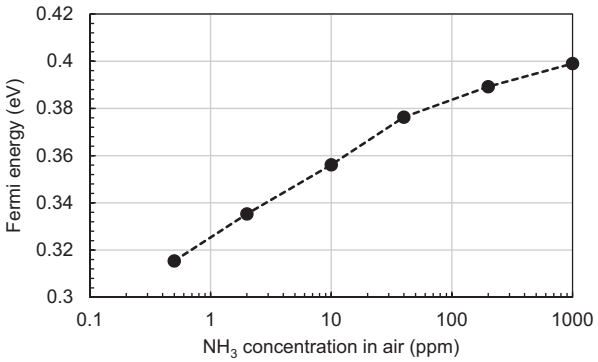

Fig. 4. The evaluated μ_c for the graphene in NH_3 atmosphere.

conductivity σ as a function of the Fermi energy μ_c using eq.(1) is plotted in Fig. 3. The μ_c for the graphene in NH_3 atmosphere is evaluated using the conductivity from Fig. 2 as shown in Fig. 4. From Figs. 3 and 4, the complex conductivity $\sigma = \sigma' + j\sigma''$ is found as in Fig. 5.

The complex refractive index $n = n' + jn''$ of the graphene is calculated from $\sigma = \sigma' + j\sigma''$

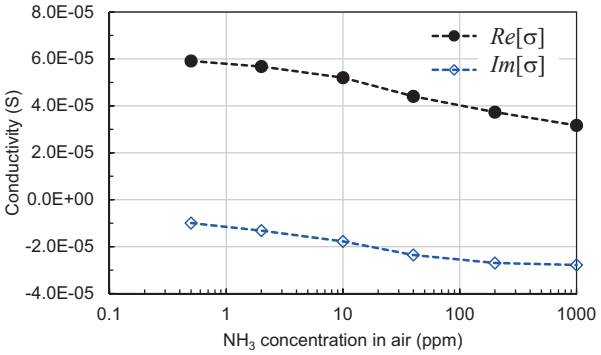

Fig. 5. The complex conductivity $\sigma = \sigma' + j\sigma''(= Re[\sigma] + jIm[\sigma])$ for the graphene in NH_3 atmosphere.

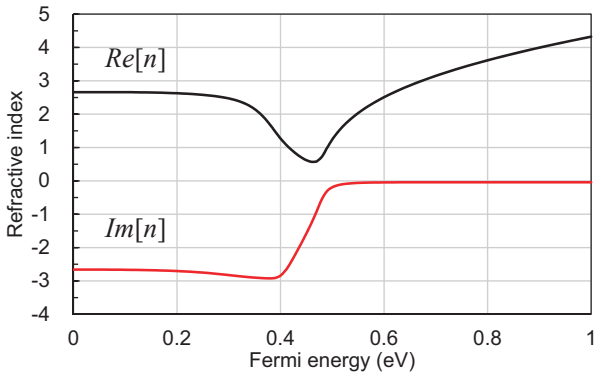

Fig. 6. The theoretical complex refractive index of graphene as a function of the Fermi energy.

by[15)]

$$n' = \sqrt{\frac{1}{2\omega\Delta\varepsilon_0}}\sqrt{\sigma'' + \sqrt{\sigma''^2 + \sigma'^2}}, \quad n'' = -\frac{\sigma'}{2\varepsilon_0\omega\Delta}\frac{1}{n'}, \tag{2}$$

where ε_0 is the dielectric constant under vacuum, Δ is the graphene thickness. We assume Δ to be 0.4 nm.[31)] Fig. 6 plots the complex refractive index as a function of the Fermi energy.

The evaluated complex refractive index of graphene as a function of NH_3 concentration in air is finally obtained as shown in Fig. 7.

Optical guided modes were analyzed by finite element method (FEM) with COMSOL software. The guided modes in silicon ridge waveguide of $W = 500$ nm and $H = 220$ nm with 0.4-nm thickness graphene cover were calculated at wavelength $\lambda = 1551.2$ nm. The thin Si layer below the Si core for voltage application was not considered in the calculation. Mesh grids in the cross-section of the waveguide for the FEM calculation are shown in Fig. 8(a), where the dense grids are used to model thin mono-layer graphene. The detailed grids at the right-lower corner of the silicon core are shown in Fig. 8(b).

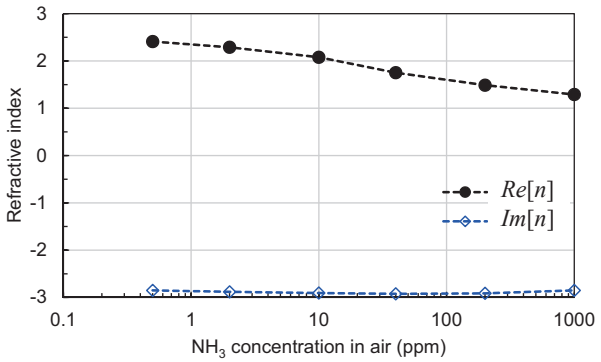

Fig. 7. The evaluated complex refractive index $n = n' + jn''(= Re[n] + jIm[n])$ of graphene as a function of NH_3 concentration.

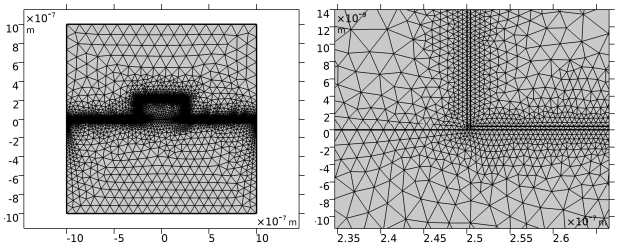

(a) (b)

Fig. 8. Mesh grids for FEM calculation, (a) modeled waveguide area and (b) at the right-lower corner of silicon core.

The x, y, and z components of the calculated electric fields in TE-like mode in the case of NH_3 gas concentration of 0.5 ppm are plotted in Figs. 9(a), (b), and (c), respectively. The total electric field $|E|$ is also plotted in Fig. 9(d).

The calculated complex effective index $N = N_r + jN_i$ of the TE-like mode is shown in Fig. 10. Both N_r and $|N_i|$ decrease with the NH_3 concentration. The decrease of $|N_i|$ means decrease of propagation loss of the guided mode.

Now, we consider the ring resonator. The transmittance of the resonator is obtained by[32)]

$$\left|\frac{E_{\text{out}}}{E_{\text{in}}}\right|^2 = \frac{r^2 + a^2 - 2ar\cos\phi}{1 + a^2r^2 - 2ar\cos\phi}, \tag{3}$$

where r is the uncoupled (bar-path) coefficient between the ring and the straight waveguide, $a = \exp(2\pi k_0 N_i R)$ corresponds to the ring propagation loss, $k_0 = 2\pi/\lambda$ is the wave number, and $\phi = -2\pi k_0 N_r R$ is the round-trip phase shift experienced in the ring. The radius R of the ring is assumed as 50 μm. We also assume the uncoupled coefficient r as 0.95. The transmittance drops at nearly periodical wavelengths. Figure 11 shows the transmitted output intensity

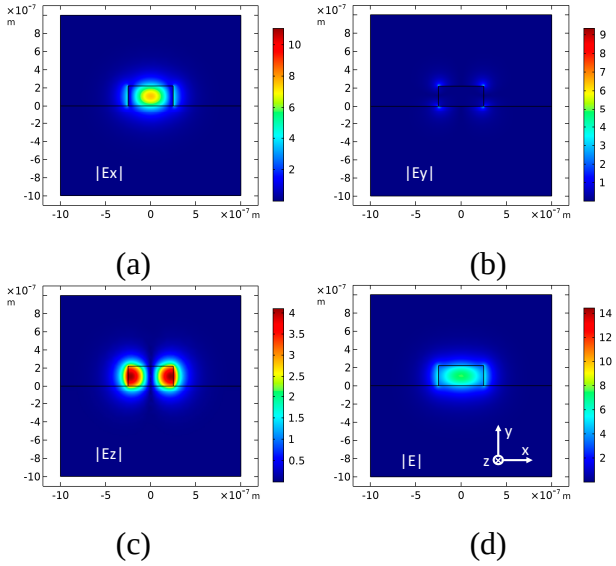

Fig. 9. Calculated electric fields in TE like mode in the case of NH_3 concentration of 0.5 ppm, (a) $|E_x|$, (b) $|E_y|$, (c) $|E_z|$, and (d) $|E|$.

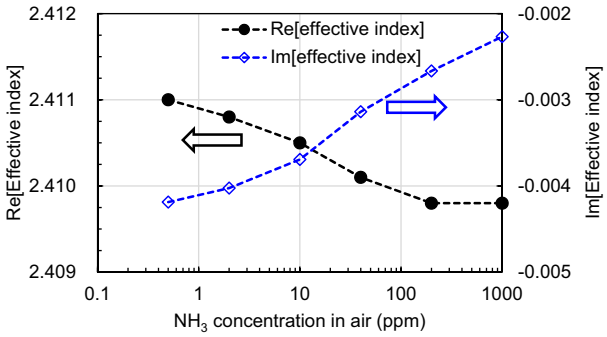

Fig. 10. Effective index $N = N_r + N_i$ of the guided TE-like mode as a function of NH_3 concentration.

$|E_{out}/E_{in}|^2$ for the cases of NH_3 concentration of 0.5, 2, 10, 40, 200, and 1000 ppm. The effective index at each of the wavelength is calculated by FEM in order to consider the wavelength dependence of N_r and N_i due to the large dispersion of Si waveguide. The minimum output intensity (dip) shifts to shorter wavelength direction by increasing the gas concentration. The resonant dip is relatively broad due to the propagation loss of the guided mode. The free spectral range (FSR) is around 1.8 nm. The Q factor is calculated to be around 1700. The Q factor without graphene overlay is calculated to be 52500 by using Eq. (20) in Ref.[33] The graphene overlay reduces the Q factor. In Ref.,[20] the Q factor for the ring resonator of $R = 10$ μm reduces from 7900 to 1200 by overlaying graphene in the length from 0 to 20 μm.

One of the wavelength drop varies as a function of NH_3 concentration as shown in Fig. 12. Thus, the gas concentration is measured by the wavelength shift of the dip. The dip wave-

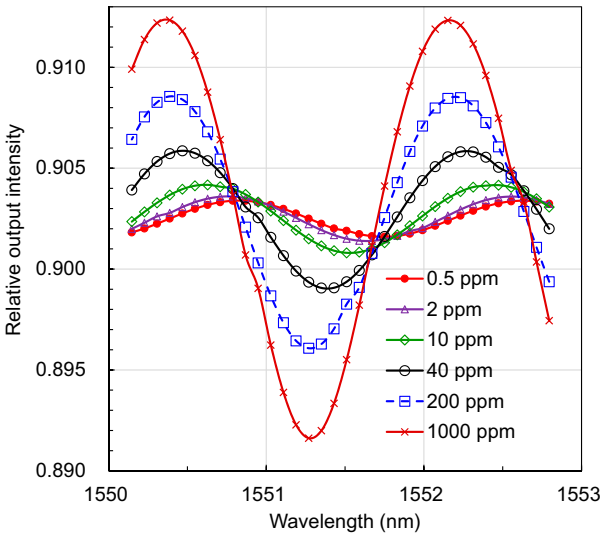

Fig. 11. Wavelength dependence of the output intensity from the resonator for NH_3 concentration of 200 ppm and 1000 ppm.

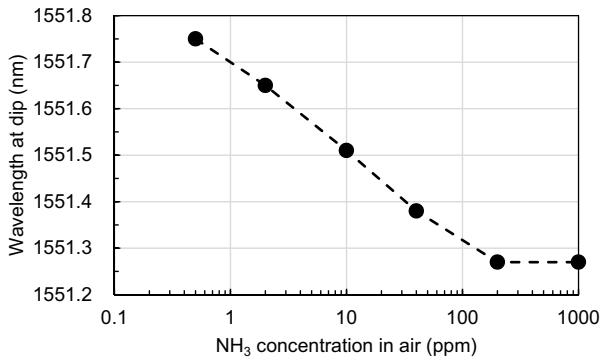

Fig. 12. The dip wavelength of the resonant as a function of the NH_3 concentration.

length decreases monotonically with the NH_3 concentration. The sensing sensitivity varies with the gas concentration. The sensitivity from 0.5 to 2 ppm is evaluated to be 67 pm/ppm, whereas the value decreases to 0.69 pm/ppm from 40 to 200 ppm.

Finally, we discuss controllability of the measurement sensitivity. The Fermi energy μ_c is changed by applying voltage to the graphene. The carrier density in the graphene is changed by applying electric voltage. This is caused by Fermi energy shift induced by carriers. The change of Fermi energy V_D is given by[14)]

$$V_D = \frac{\hbar v_F}{q}\sqrt{\frac{\pi\varepsilon V_g}{qd}}, \tag{4}$$

where v_F is the Fermi velocity (=106 m/s), $\varepsilon/\varepsilon_0$ for SiO_2 is 3.8. Fig. 13(a) shows the cal-

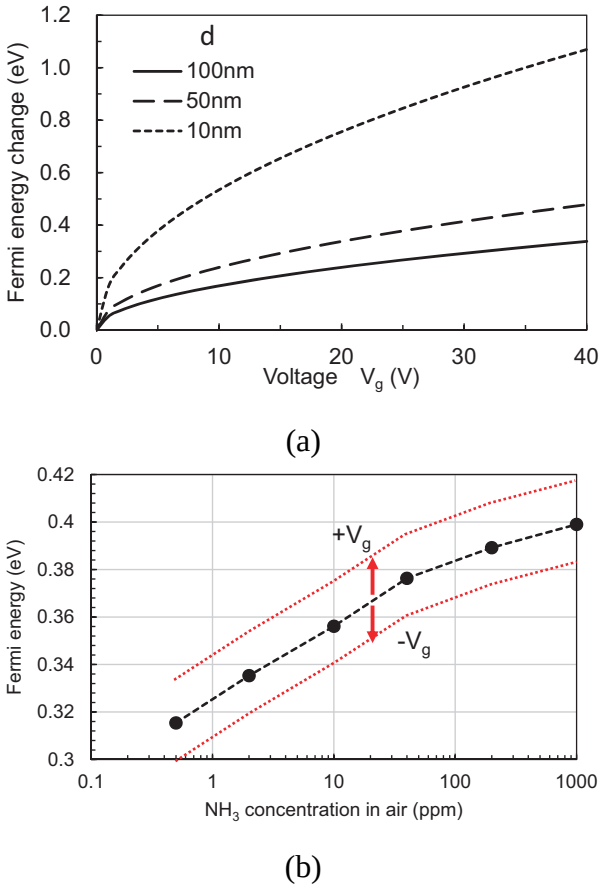

Fig. 13. Adjustment of sensitivity by applying voltage V_g; (a) Fermi energy change by applying voltage to graphene, (b) Fermi energy change as a function of NH_3 concentration.

culated V_D with SiO_2 thickness d as a parameter. The Fermi energy as a function of NH_3 concentration shown in Fig. 4 is expected to be adjusted by applying the voltage V_g as illustrated in Fig. 13(b). The sensitivity for higher NH_3 concentration might be adjusted by applying a negative voltage V_g according to the gas concentration range to be measured. Note that the sign of q is changed with the sign of V_g since the dominant carrier for the negative voltage case is hole.[34)]

4. Conclusion

An optical NH_3 gas sensor consisting of graphene covered microring resonator was proposed. The sensitivity was analyzed by FEM. It was clarified from the simulation using experimental data on graphene resistivity that the gas concentration from 0.5 to 1000 ppm was successfully measured by the resonant wavelength shift of the microring resonator. The sensitivity from 0.5 to 2 ppm was evaluated to be 67 pm/ppm. The sensitivity of the gas detection might be adjusted by applying electric voltage to the graphene to shift its Fermi energy. There is

a trade-off between the sensitivity and the extinction ratio calculated from the spectral dip depth at the resonant wavelength due to the relation of graphene length and optical loss. Although the required sensitivity and extinction ratio depend on the application, we will consider optimized designs and performances for the proposed optical NH_3 gas sensor. We will also numerically evaluate the resonator characteristics of the proposed sensor in future by using finite difference time domain method.

References

1) A. K. Geim and K. S. Novoselov, Nature Materials, **6**, 183 (2007).
2) K. S. Novoselov, V. I. Fal'ko, L. Colombo, P. R. Gellert, M. G. Schwab, and K. Kim, Nature, **490**, 192 (2012).
3) B. Sensale-Rodriguez, J. Lightwave Technol., 33, 1100 (2015).
4) F. Schedin, A. K.Geim, S. V. Morozov, E. W. Hill, P. Blake, M. I. Katsnelson, and K. S. Novoselov, Nature Materials, **6**, 652 (2007).
5) O. Leenaerts, B. Partoens, and F. M. Peeters, Phys. Rev. B, **77**, 125416 (2008).
6) M. Harnaez, C. R. Zamarreno, S. Melendi-Espina, L. R. Bird, A. G. Mayes, and F. J. Arregui, Sensors, **17**, 155 (2017).
7) Y. Zhao, X.-G. Li, X. Zhou, Y.-N. Zhang, Sensor and Actuators B, **231**, 324 (2016).
8) B. N. Shivananju, W. Yu, Y. Liu, Y. Zhang, B. Lin,S.Li, and Q. Bao, Advanced Functional Materials, **27**, 19, 1 (2017).
9) Y. Wu, B. Yao, C. Yu, and Y. Rao, Sensors, **18**, 941 (2018).
10) S. S. Varghese, S. Lonkar, K. K. Singh, S. Swaminathan, and A. Abdala, Sensors and Actuators B, **218**, 160 (2015).
11) Y. Dan, Y. Lu, N. J Kybert, Z. Luo, and A. T. C. Johnson, Nano Letters, **9**, 1472 (2009).
12) G. Ko, H.-Y. Kim, J. Ahn, Y.-M. Park, K.-Y. Lee, and J. Kim, Current Applied Physics, **10**, 1002 (2010).
13) R. Kumar, R. Singh, D. Hui, L. Feo, F. Fraternali, Composites, Part B, **134**, 193 (2018).
14) A. Maliakal, L. Reith, and S. Cabot, Appl. Phys. Lett., **108**, 153109 (2016).
15) B. Yao, Y. Wu, Y. Cheng, A. Zhang, Y. Gong, Y.-J. Rao, Z. Wang, and Y. Chen, Sensors and Actuators B, **194**, 142 (2014).
16) T. Hao and K. S. Chiang, IEEE Photonic. Tech. Lett. **29**, 2035 (2017).
17) H. Fu,Y.Jiang, J. Ding, J. Zhang, M. Zhang, Y. Zhu, H. Li, Sensor and Actuators B, **254**, 239 (2018).
18) Y. Wu, B.-C. Yao, Y. Cheng, Y.-J. Rao, Y. Gong, W. Zhang, Z. Wang, and Y Chen, IEEE J. Selected Topics in Quantum Electronics, **20**, 4400206 (2014).
19) Q. Bao, H. Zhang, B. Wang, Z. Ni, C. Haley, Y. X. Lim, Y. Wang, D. Y. Tang, and K. P. Loh, Nature Photonics, **5**, 411 (2011).
20) R. Kou, S. Tanabe, T. Tsuchizawa, T. Yamamoto, H. Hibino, H. Nakajima, and K. Yamada, Appl. Phys. Lett., **104**, 091122 (2014).
21) C. Qiu, W. Gao, R. Vajtai, P. M. Ajayan, J. Kono, and Q. Xu, Nano Lett., **2014**, 6811

(2014).

22) W. Bogaerts, P. De Heyn, T. Van Vaerenbergh, K. De Vos, S. K. Selvaraja, T. Claes, P. Dumon, P. Bienstman, D. Van Thourhout, and R. Baets, Laser Photonics Rev., **6**, 47 (2012).

23) A. F. Gavela, D. G. Garcia, J. C. Ramirez, and L. M. Lechuga, Sensors, **16**, 285 (2016).

24) K. De Vos, I. Bartolozzi, E. Schacht, P. Bienstman, and R. Baets, Opt. Exp., **15**, 7610 (2007).

25) M. K. Park, J. S. Kee, J. Y. Quah, V. Netto, J. Song, Q. Fang, E. M. La Fosse, G.-Q. Lo, Sensors and Actuators B, **176**, 552 (2013).

26) M. Sato, H. Kishikawa, N. Goto, S. Yanagiya, and S.-K. Liaw, 23rd MicroOptics Conference (MOC2018), Taipei, P-68 (2018).

27) Y. Wu, B. Yao, C. Yu, and Y. Rao, Sensors, **18**, 941, (2018).

28) B. Timmer, W. Olthuis, and A. V. D. Berg, Sensors and Actuators B, **107**, 666, (2005).

29) F. Yavari, E. Castillo, H. Gullapalli, P. M. Ajayan, and N. Korathar, Appl. Phys. Lett., **100**, 203120 (2012).

30) Y.-C. Chang, C.-H. Liu, C.-H. Liu, Z. Zhong, and T. B. Norris, Appl. Phys. Lett., **104**, 261909 (2014).

31) Y. Yao, L. Ren, S. Gao, and S. Li, J. Materials Science and Technology, **33**, 815 (2017).

32) J. E. Heebner, V. Wong, A. Schweinsberg, R. W. Boyd, and D. J. Jackson, IEEE J. of Quantum Electron., **40**, 726 (2004).

33) W. Bogaerts, P. D. Heyn, T. V. Vaerenbergh, K. D. Vos, S. K. Selvaraja, T. Claes, P. Dumon, P. Bienstman, D. V. Thourhout, and R. Baets, Laser and Photonics Reviews, **6**, 47, (2012).

34) Z. Q. Li, E. A. Henriksen, Z. Jiang, Z. Hao, M. C. Martin, P. Kim, H. L. Stormer, and D. N. Basov, Nature Physics, **4**, 532, (2008).